difference between theory and experiment can be ascribed to a breakdown of the effective-mass approximation. For the electric and magnetic fields that we applied, $(eEa_L/\hbar\omega_v)$ is smaller than 0.1 for the light holes, but it becomes of order 1 for the heavy holes. Therefore, the heavy holes cannot be treated in the effective-mass approximation. It is probable that for these high values of electric field, discrete levels no longer exist for the heavy holes, which would explain the fact that we do not observe any peaks in the absorption spectra that can be attributed to heavy-hole–electron transitions. It would certainly be meaningless to try to include the heavy holes in a calculation of the type developed in Sec. IV, which assumes the effective-mass approximation to hold.

Our results can be summarized as follows. Three interband magneto-optical transitions have been observed in germanium at energies below the direct gap in the presence of a large electric field perpendicular to the magnetic field. One of these transitions is a forbidden one, induced by the electric field, whereas others are allowed transitions. The shift of the transition energies due to the electric and magnetic fields as well as the intensity behavior have been studied. From the experimental data the energies of three light-hole levels in crossed electric and magnetic fields have been determined in a range of E/H values for which perturbation theories developed earlier are not valid (the requirement $eEL_M/\hbar\omega_v \ll 1$ is not fulfilled). The theory, which goes beyond the perturbation treatment, was developed within the framework of the effective-mass approximation by neglecting the electric-field-induced interaction between the light holes and heavy holes. The theory is in satisfactory agreement with the experimental data. It accounts in particular for the observation that the electric field removes the quantum effects from the light-hole Luttinger ladders.

ACKNOWLEDGMENTS

The authors are grateful to Professor Benjamin Lax for his interest in their work, to Dr. A. Frova and Professor P. Handler of the University of Illinois for kindly providing the germanium diodes used in the experiments, and to R. E. Newcomb for assistance with the measurements.

PHYSICAL REVIEW VOLUME 158, NUMBER 3 15 JUNE 1967

Nonlocal Effects in Low-Field Helicon Propagation in PbTe†

J. N. WALPOLE* AND A. L. MCWHORTER
Lincoln Laboratory‡ and Electrical Engineering Department, Massachusetts Institute of Technology, Cambridge, Massachusetts

(Received 28 December 1966)

Helicon propagation has been studied in the region of low magnetic fields, where band structure and nonlocal Landau damping effects produce sizable corrections to the high-field dispersion relation. Good agreement with both the phase and amplitude of 9-GHz helicons in n-PbTe at 4.2°K is obtained by a semiclassical treatment of a degenerate, many-valley, ellipsoidal model. The calculation is carried out by expanding the conductivity tensor in powers of $1/B_0$, treating ω/ω_c, $1/\omega_c\tau$, and qv_F/ω_c as small quantities, where B_0 is the static magnetic field, ω_c is the cyclotron frequency, τ is the collision time, q is the wave number, and v_F is the Fermi velocity. Because of the anisotropic energy surfaces in PbTe, Landau damping occurs for propagation along the field as well as at an angle. The corrections to the phase are quite sensitive to the transverse effective mass; comparison with experiment yields a value of $0.020m_0$ for the band-edge transverse mass in PbTe. It is also found that both relaxation to the local equilibrium and anisotropic scattering are important effects, although only the former is included in the theoretical calculations.

I. INTRODUCTION

IN a sufficiently large static magnetic field, it is possible for circularly polarized electromagnetic waves to propagate with negligible damping in conducting solids. These waves, known as helicons, have been studied in many metals and semiconductors.[1] Provided that displacement current and quantum effects can be neglected, the helicon dispersion relation in high magnetic fields is independent of band structure and depends only on the carrier concentration, the strength of the magnetic field, and the angle of the field with

† Based on a thesis submitted by J. N. Walpole to the Massachusetts Institute of Technology in partial fulfillment of the requirements for the degree of Doctor of Philosophy.

* National Science Foundation Graduate Fellow during a portion of this work.

‡ Operated with support from the U. S. Air Force.

[1] For reviews of theoretical and experimental work on helicons see articles by S. J. Buchsbaum, in *Plasma Effects in Solids* (Dunod Cie., Paris, 1965), p. 3; R. Bowers, *ibid.*, p. 19. Alfvén waves propagate instead of helicons if the concentration of holes and electrons are equal.

respect to the direction of propagation. The aim of the present work is to investigate the low-field behavior of helicons where corrections to the phase and amplitude depend strongly on band structure and nonlocal conductivity effects. Microwave transmission experiments have been carried out at 9 GHz on n-type lead telluride at 4.2°K and in magnetic fields between 0.7 and 10 kG. The model of a many-valley degenerate semiconductor with ellipsoidal energy surfaces is treated in some detail and yields good agreement with the experimental results.

The helicon dispersion relation in high magnetic fields (but not so large that displacement current or quantum effects need be included) is[1]

$$q=\left(\frac{ne\omega\mu_0}{B_0\cos\theta}\right)^{1/2}, \tag{1.1}$$

where q is the wave number, ω the wave frequency, e the electronic charge, μ_0 the permeability of free space, n the carrier concentration, B_0 the static magnetic field, and θ the angle between $\mathbf{q}$ and $\mathbf{B}_0$. The helicon is often called an ac manifestation of the Hall effect since (1.1) may be derived from Maxwell's equations assuming that the motion of the carriers is dominated by the Lorentz force. In the high-field limit the current density and electric field vectors are at all times perpendicular and there is no dissipation or damping of the wave. The expression for q given in (1.1) will be called the zeroth-order expression and henceforth denoted by q_0. More precisely, (1.1) is obtained from the complete expression when terms of order ω/ω_c, $1/\omega_c\tau$, and qv_F/ω_c are neglected in comparison with unity, where ω_c is the cyclotron frequency, τ is the collision time and v_F is the Fermi velocity. The neglect of displacement current requires that $ne/B_0\gg\omega\epsilon_L$, where ϵ_L is the lattice dielectric constant.[2]

In this paper we consider the low-field behavior of helicons where ω/ω_c, $1/\omega_c\tau$, and qv_F/ω_c are not so small that they may be neglected, but yet sufficiently small that corrections to q_0 up to second order in these quantities may be calculated by an expansion of the conductivity tensor in powers of $1/B_0$. The corrections thus introduced depend strongly on band structure and the degree to which the current–electric-field relation within the sample is described by a local (wave-vector-independent) conductivity or by a nonlocal (wave-vector-dependent) conductivity.

In the nonlocal regime, two types of resonant (collisionless) damping, accompanied by strong effects on the phase, may occur. These are Doppler-shifted cyclotron resonance (DSCR) and Landau damping. The former, which has been widely studied,[3–7] will not be discussed in detail here since it occurs when $qv_F/\omega_c\sim1$, a condition not reached in the present experiments.

Landau damping, however, may occur at higher fields where qv_F/ω_c may be treated as a small quantity. It is a resonant interaction with the wave by particles whose average velocity over the cyclotron orbit has a component along the direction of propagation equal to the wave velocity.[8,9] Landau damping, originally predicted for helicon waves by Kaner and Skobov,[10] has been observed for helicons propagating at an angle to the magnetic field in alkali metals by Grimes[11] and by Houck and Bowers.[12] Although the treatment by Kaner and Skobov predicts no damping for propagation along the magnetic field, this result is correct only for special symmetry of the Fermi surface. In particular, for ellipsoidal energy surfaces with propagation parallel to B_0 but not along a principal axis of the ellipsoid, the damping is not zero.

Just such a situation is encountered in the present experiments on lead telluride, which show Landau damping for propagation along the field as well as at an angle. Comparison will be made between theory and experiment using both local and nonlocal conductivity tensors in order to show the size of the nonlocal corrections that are involved. The mechanism through which energy is transferred from the wave to the resonant particles is not discussed here, however; this matter is treated in the following paper[9] in a more general context for a closed Fermi surface of arbitrary shape.

II. EXPERIMENTAL TECHNIQUES

The phase and amplitude of 9-GHz microwave signals transmitted by helicon waves through samples of n-PbTe were measured at 4.2°K as the magnitude and orientation of the static magnetic field were varied. The microwave system used was originally assembled by May and has been described elsewhere.[13] Two signals are transmitted from the source to the receiver. One is modulated and passes through the sample; the other, the "feed-around" signal, is unmodulated, larger than

[2] For the range of magnetic fields and carrier concentrations used in the present experiments, displacement current may be neglected even though ϵ_L is unusually large in PbTe. [W. Cochran, Phys. Letters **13**, 193 (1964).]

[3] E. A. Stern, Phys. Rev. Letters **10**, 91 (1963).

[4] M. T. Taylor, Phys. Rev. **137**, A1145 (1965).

[5] A. W. Overhauser and S. Rodriguez, Phys. Rev. **141**, 431 (1966).

[6] J. C. McGroddy, J. L. Stanford, and E. A. Stern, Phys. Rev. **141**, 437 (1966).

[7] J. L. Stanford and E. A. Stern, Phys. Rev. **144**, 534 (1966).

[8] For reasons discussed in the following paper (Ref. 9) we use the term Landau damping to include the effect of all field components in producing the resonant transfer of energy.

[9] A. L. McWhorter and J. N. Walpole, following paper, Phys. Rev. **158**, 719 (1967).

[10] E. A. Kaner and V. G. Skobov, Zh. Eksperim. i Teor. Fiz. **45**, 610 (1963) [English transl.: Soviet Phys.—JETP **18**, 419 (1964)].

[11] C. C. Grimes, Bull. Am. Phys. Soc. **11**, 570 (1966).

[12] J. R. Houck and R. Bowers, Bull. Am. Phys. Soc. **11**, 256 (1966).

[13] A. L. McWhorter and W. G. May, IBM J. Res. Develop. **8**, 285 (1964); W. G. May, Ph.D. thesis, Massachusetts Institute of Technology, 1964 (unpublished).

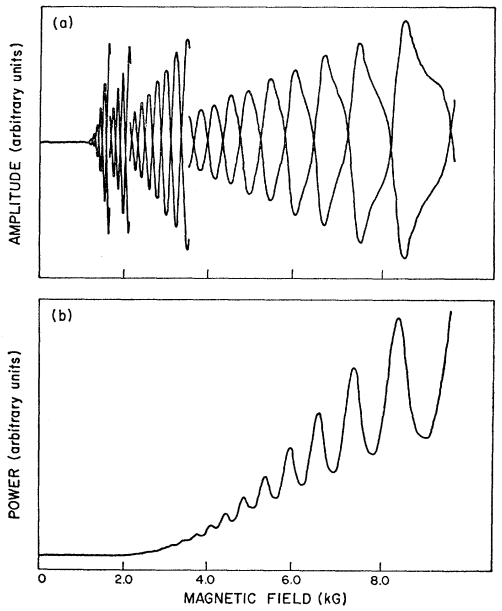

FIG. 1. Typical recorder traces of the receiver output versus magnetic field illustrating (a) interferometer mode, in which the amplitude and phase of the transmitted signal is measured using a "feed-around" signal, and (b) simple detection of the transmitted power using no feed-around. The phase of the feed-around signal differs by 180° in the two superimposed traces in (a); the discontinuities in the amplitude result from successively adding 12 dB attenuation in the sample arm.

the modulated signal transmitted through the sample, and has a calibrated phase shifter and attenuator in its path. The interference between the two signals can be used to measure phase just as with the "leakage" technique,[14,15] while in addition a sensitivity of 10^{-20} W can be achieved by synchronously detecting at the modulation frequency. Furdyna[16] has also used a "controlled leakage" system for helicon experiments, but without the sensitivity of modulation and synchronous detection. Interference patterns of the type obtained by Furdyna[16] were used to determine the amplitude and phase delay of the transmitted signal, as illustrated in Fig. 1(a). Two superimposed recorder traces of the receiver output versus magnetic field are shown, the two traces corresponding to a 180° difference in the setting of the phase shifter in the feed-around arm. The helicon phase delay is obtained from the position of the nulls, which occur at intervals of 180°; the amplitude is determined from the envelope of the traces.

The lower trace, Fig. 1(b), shows the receiver output without the feed-around signal. The oscillations here are the dimensional resonances due to multiple reflections of the helicon from the sample faces. The effect of these dimensional resonances is seen in Fig. 1(a) as a distortion of the interference pattern at high fields. Without feed-around the output of the receiver is proportional to the power in the transmitted signal.

In addition to the recorder traces, a point-by-point measurement of the phase and amplitude of the signal was sometimes used, particularly for measuring the change in phase and amplitude as the direction of the magnetic field was rotated with respect to the direction of propagation. By nulling the signal, the phase could be determined with a precision of about ±1 degree at moderate signal levels. The angle between the field and the direction of propagation was measured to 0.1°.

The mounting arrangement of the samples is shown in Fig. 2. The sample, which is plated with gold and copper around its edges as described later, is soldered over a circular iris in a copper-plated magnesium plate. Plating is used on both the sample and the magnesium plate so that solder joints are easily made and reliably microwave tight. This plate is then "sandwiched" between two thicker magnesium plates with indium gaskets inserted as shown in the figure. The indium gaskets prevent microwave leakage from the joints. Magnesium is used in the thin plate and the two thicker ones as a precaution against thermal stress. The total thermal contraction of this material from room temperature to liquid-helium temperature closely matches that of PbTe.[17] Finally the set of plates and gaskets are bolted between two brass flanges with circular ridges which again prevent leakage of microwave signals.

The incident microwave signal travels toward the sample through an essentially smooth and continuous rectangular waveguide, which is shorted at the end by the sample and the magnesium mounting plate. The bends occurring on each side of the sample have a low reflection coefficient, and the sample and other irregularities in the mounting arrangement are of small size

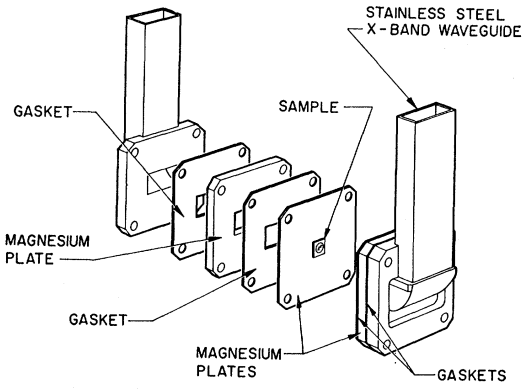

FIG. 2. Mounting arrangement of sample between waveguide flanges. Indium gaskets are used to prevent leakage of the microwave signal; magnesium is used for the mounting and supporting plates because its thermal contraction approximately matches that of PbTe.

[14] G. A. Williams and G. E. Smith, IBM J. Res. Develop. **8**, 276 (1964).
[15] C. C. Grimes, Bull. Am. Phys. Soc. **9**, 239 (1964).
[16] J. K. Furdyna, Phys. Rev. Letters **14**, 635 (1965); Rev. Sci. Instr. **37**, 462 (1966).
[17] S. I. Novikova and N. K. Abrikosov, Fiz. Tverd. Tela **5**, 1913 (1963) [English transl.: Soviet Phys.—Solid State **5**, 1397 (1964)].

compared to the wavelength of the radiation in the guide. Because of the high conductivity of the PbTe, the surface of the sample is essentially at a node of the electric field, with the magnetic field being twice that of the incident wave. Since the sample is small and located in the center of the guide, the magnetic field is very nearly uniform across the surface and linearly polarized in the plane of the surface. By using the continuity of H across the boundary, the excitation of the propagating helicon mode can be determined. Similar considerations apply at the other sample-waveguide interface, which appears as an open circuit to the propagating wave.

Inside the sample, because of its high effective dielectric constant, wavelengths will be extremely small ($\sim 40\mu$) and it is a good approximation to treat the sample as infinite in the directions perpendicular to the propagation direction. That is, diffraction effects may be neglected provided the wide dimensions of the sample are large compared to the wavelength. Thus a simple plane wave propagating perpendicular to the surface is excited. The surfaces of the sample must be flat and parallel to at least a quarter of the wavelength to prevent interference effects.

Before the final mounting of the samples, a somewhat lengthy and careful preparation procedure was followed. PbTe is extremely susceptible to cracking and cleaving. It is also quite soft and therefore easily scratched and damaged by working, grinding, and cutting. Hence it is necessary to use techniques which avoid mechanical and thermal shocks to the material.

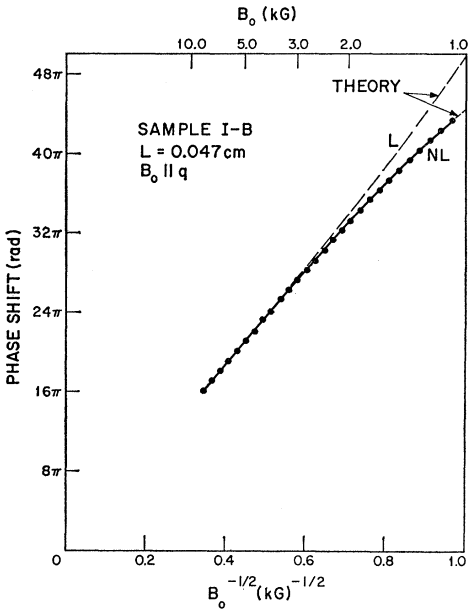

FIG. 3. Phase delay of the helicon wave versus $B_0^{-1/2}$ for sample *I-B* with the magnetic field along the propagation direction. Points are experimental; curves labeled *L* and *NL* are calculated using local and nonlocal conductivity tensors, respectively. The sample thickness is 0.047 cm and the carrier concentration is 8.1×10^{17} cm^{-3}.

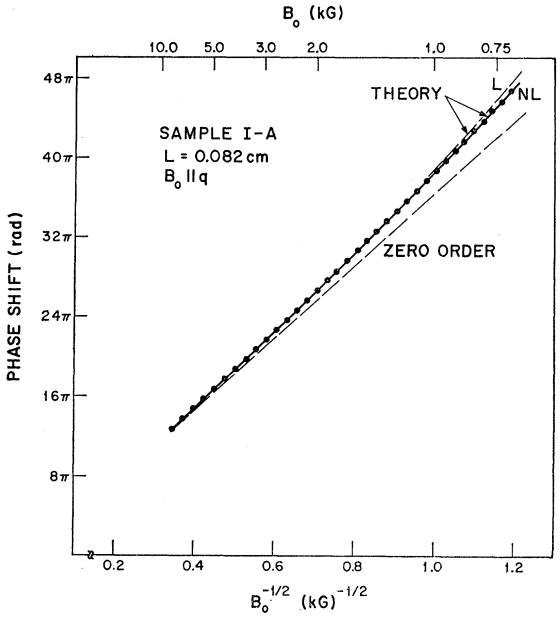

FIG. 4. Phase delay of the helicon wave versus $B_0^{-1/2}$ for sample *I-A* with the magnetic field along the propagation direction. Points are experimental; curves labeled *L* and *NL* are calculated using local and nonlocal conductivity tensors, respectively. The zeroth-order curve neglects both band structure and nonlocal corrections. The sample thickness is 0.082 cm, and the carrier concentration is 1.7×10^{17} cm^{-3}.

Starting material was an as-grown (Bridgeman furnace), *p*-type ingot obtained from Battelle with $p\simeq 2\times10^{18}$ cm^{-3} and $\mu\simeq 200{,}000$ cm^2/volt sec at $T=4.2$°K. Wafers oriented in the (100) direction and approximately 0.1 cm thick were cut from the ingot using a spark erosion cutter which applies no mechanical force. After the work damage was removed by grinding and etching,[18] the samples were annealed by a procedure similar to that used by Brebrick and Gubner.[19] The purpose of the annealing procedure is to produce a controlled deviation from stoichiometry and thus adjust carrier type and concentration. In addition, the high temperatures used (600 to 750°C) may relieve strains to some extent. After annealing, the samples were ground to the desired thickness and then etched to achieve a polished surface. The sample faces remained smooth and parallel if the final etching was kept to a minimum.

Next a thin gold film was evaporated on the samples except for circular areas about 0.2 cm in diameter through which the signal was to be transmitted. Copper was then electroplated on the gold, and finally another film of gold was evaporated on the copper to improve wetting of the indium solder to the sample during the final soldering operation of the sample to the magnesium card. The copper plating provides a thick

[18] M. K. Norr, U. S. Naval Ordnance Laboratory Report No. T. R. 63-156, 1963 (unpublished).

[19] R. F. Brebrick and E. Gubner, J. Chem. Phys. **36**, 1283 (1962).

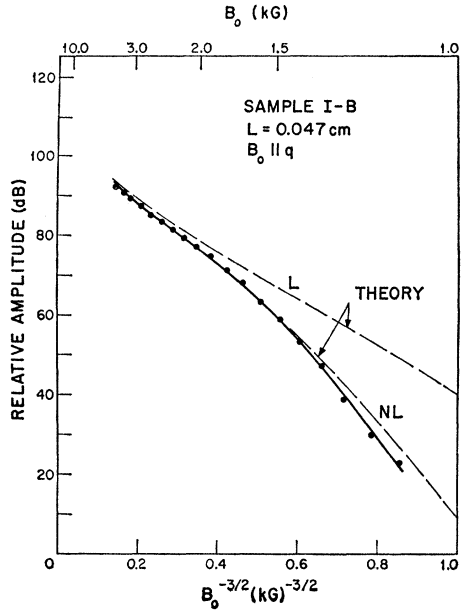

FIG. 5. Transmitted amplitude of the helicon wave versus $B_0^{-3/2}$ for sample *I-B* with the magnetic field along the propagation direction. Solid curve through points is experimental. Dashed curves labeled *L* and *NL* are calculated using local and nonlocal conductivity tensors, respectively.

base which does not dissolve into the solder, thus preventing an alloy forming between the PbTe and the indium, which otherwise would have cracked the sample because of differences in thermal contraction.

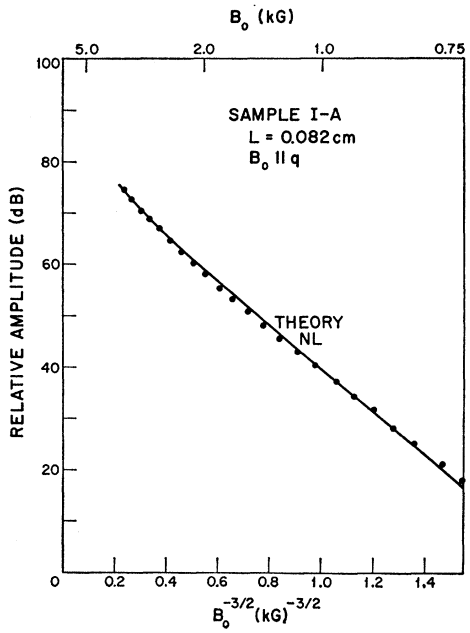

FIG. 6. Transmitted amplitude of the helicon wave versus $B_0^{-3/2}$ for sample *I-A* with the magnetic field along the propagation direction. Points are experimental. Solid curve labeled *NL* is calculated using a nonlocal conductivity tensor.

III. EXPERIMENTAL RESULTS

The phase-shift plots for two samples of different concentration are shown in Fig. 3 and Fig. 4. For both samples the magnetic field is along the [001] axis which is the direction of propagation. The theoretical curves labelled *L* for local and *NL* for nonlocal conductivity were calculated as described in the next section. The experimental points lie almost exactly on the *NL* curves. In Fig. 4 the zeroth-order dispersion line given by (1.1) is also shown for comparison.

Sample *I-B* in Fig. 3 has the higher concentration, $n=8.1\times10^{17}$ cm^{-3}, and shows strong nonlocal behavior. Sample *I-A* in Fig. 4 has a concentration of 1.7×10^{17} cm^{-3}, and is only slightly affected by the nonlocal correction. A similar behavior is noted in the amplitude data shown in Fig. 5 and Fig. 6. In the first of these figures the nonlocal correction is appreciable. In the second there is little difference in the theoretical curves for the local and nonlocal regimes and only the latter is shown.

For propagation at an angle to the field, the change in phase and the change in amplitude of the transmitted signal as a function of angle were measured as described in the preceding section. The field was held constant in magnitude and rotated in the (100) plane. The results for sample *I-B* are compared to theoretical curves for both the local and nonlocal regimes in Fig. 7. The graph of phase shift also shows the zeroth-order contribution which is due to the angular dependence of q_0 in (1.1). In Fig. 8 the results for sample *I-A* are compared to theoretical calculations for the nonlocal theory only, since again the local calculation yields essentially the same curve. It should be noted that the only serious discrepancy between the experimental results and the theory occurs in the curves for change in amplitude with the angle of the magnetic field. As will be discussed later, this disagreement is believed to be due to anisotropic scattering, which was not included in the calculation.

Results similar to those shown in Figs. 3–8 were obtained for two intermediate concentrations, $n=6.6\times10^{17}$ cm^{-3} and $n=4.1\times10^{17}$ cm^{-3}. A consistent trend toward stronger nonlocal effects with higher concentrations was found; comparison with theory showed the same general agreement in the phase and amplitude for the field along the propagation direction and the same disagreement in the change in amplitude with the angle of the field.

We shall return to Figs. 3–8 for further comment and interpretation after presenting the theory in the next section. The mass parameters and the concentrations and collision times used in the theoretical calculations will also be discussed later.

IV. THEORY

The dispersion relation for helicon waves in the infinite medium is obtained from the solution to

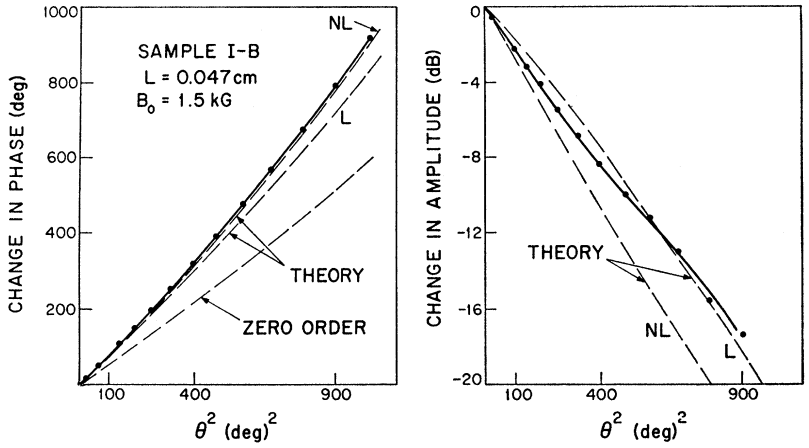

FIG. 7. Changes in the phase and amplitude of the helicon wave versus the square of the angle θ between the magnetic field and the propagation direction for sample *I-B*. The magnitude of the field is held constant at 1.5 kG. The solid curves are drawn through the experimental points; the dashed curves labeled *L* and *NL* are calculated using local and nonlocal conductivity tensors, respectively. The zeroth-order curve neglects both band structure and nonlocal corrections.

Maxwell's equations with the constitutive relation

$$\mathbf{J}=\boldsymbol{\sigma}(\omega,\mathbf{q},\mathbf{B}_0)\cdot\mathbf{E}, \tag{4.1}$$

where the conductivity tensor $\boldsymbol{\sigma}$ is generally a function of frequency, wave vector, and static magnetic field. The semiclassical conductivity tensor obtained from the solution of the Boltzmann equation[20,21] will be used here for the calculation of helicon propagation in the nonlocal regime. When ω/ω_c, $1/\omega_c\tau$ and qv_F/ω_c are all small compared to unity, as is the case in the present experiments, exact expressions for the conductivity tensor are not needed. It is sufficiently accurate to expand $\boldsymbol{\sigma}$ in powers of $1/B_0$ and keep only the leading terms. Before carrying out such a treatment, however, we shall use the form of the conductivity tensor to discuss nonlocal effects in a more general way.

A. Nonlocal Effects

The semiclassical conductivity tensor for the case of spherical energy surfaces and in the absence of spatial bunching of particles[20] is

$$\boldsymbol{\sigma}=\tfrac{3}{2}\sigma_0\sum_{n=-\infty}^{\infty}\int_0^{\pi}\frac{\mathbf{O}J_n(\xi)\mathbf{O}^{\dagger}J_n(\xi)\sin\theta d\theta}{1-i(n\omega_c-\omega+q_zv_F\cos\theta)\tau}, \tag{4.2}$$

where the vector operator $\mathbf{O}$ is given by

$$\mathbf{O}=\begin{bmatrix} n/X \\ -i\partial/\partial X \\ \cos\theta \end{bmatrix}, \tag{4.3}$$

and where $X=q_xv_F/\omega_c$ and $\xi=X\sin\theta$. The variable of integration θ is the polar angle in velocity space. The J_n are Bessel functions of integer order n and σ_0 is the dc conductivity $ne^2\tau/m$. The coordinate system used in (4.2) is such that the z axis is along the *dc* magnetic field and the x axis is chosen so that $\mathbf{q}$ lies in the xz plane and has the components q_x and q_z. When density fluctuations are present, $\boldsymbol{\sigma}$ must be replaced by a more general tensor, denoted by $\boldsymbol{\sigma}'$ in the notation of Ref. 20. The tensor $\boldsymbol{\sigma}'$, which may be expressed[20] in terms of $\boldsymbol{\sigma}$,

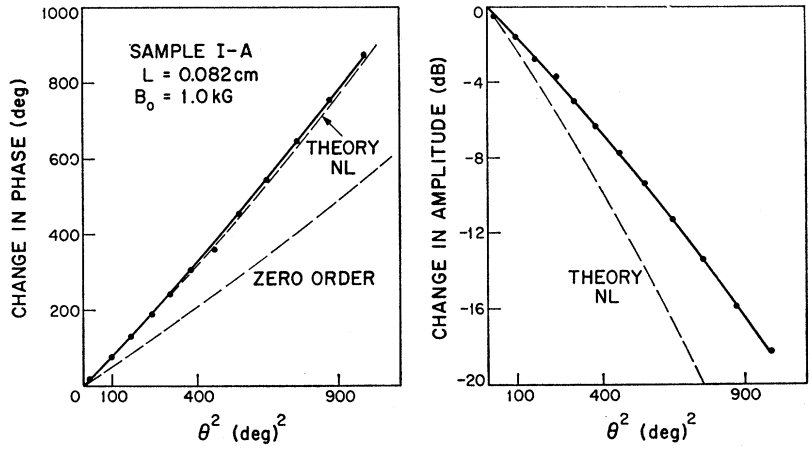

FIG. 8. Changes in the phase and amplitude of the helicon wave versus the square of the angle θ between the magnetic field and the propagation direction for sample *I-A*. The magnitude of the field is held constant at 1.0 kG. The solid curves are drawn through the experimental points; the dashed curves labeled *NL* are calculated using a nonlocal conductivity tensor. The zero-order curve neglects both band structure and nonlocal corrections.

[20] M. H. Cohen, M. J. Harrison, and W. A. Harrison, Phys. Rev. **117**, 937 (1960).
[21] S. Rodriguez, Phys. Rev. **112**, 80 (1958).

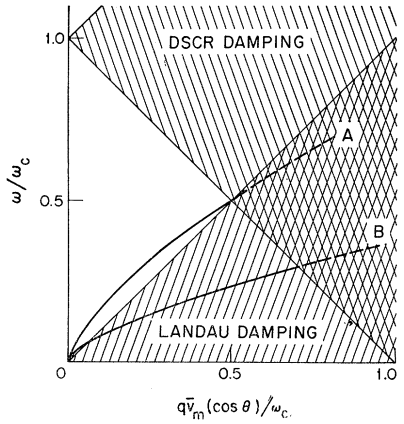

FIG. 9. Normalized ωq plane in which two zero-order helicon dispersion relations are plotted for varying magnetic field strength with the frequency and angle θ of propagation with respect to the field held constant. Resonant damping occurs in the cross-hatched regions. Curve A shows the critical case in which DSCR and Landau damping set in at the same magnetic field. Curve B corresponds to sample I-B with propagation along $\mathbf{B}_0$ and parallel to the [001] axis; in this case Landau damping occurs first as the magnetic field is decreased. The quantity $\bar{v}_m$ is the maximum average Fermi velocity along the magnetic field. In general a different dispersion relation would have to be drawn for each ellipsoid because of the normalization.

includes the effect of relaxation to the local equilibrium. However, $\boldsymbol{\sigma}'=\boldsymbol{\sigma}$ in the limit $\tau\rightarrow\infty$, so that the collisionless damping effects in the nonlocal regime may be predicted on the basis of (4.2) alone. Although perturbation calculations in the local limit[22] indicate that for finite τ the effect of collision anisotropy may be important, especially in the amplitude of the helicon wave, only isotropic collisions will be considered here. A more general treatment of collisions in the nonlocal regime introduces considerable mathematical complexity.

The use of (4.2) is not restricted to the case of spherical energy surfaces. As is well known, for an ellipsoidal Fermi surface of the form

$$E_F=\tfrac{1}{2}\mathbf{p}\cdot\mathbf{m}^{-1}\cdot\mathbf{p}, \tag{4.4}$$

the transformations

$$\begin{aligned}&\mathbf{p}=\mathbf{m}^{1/2}\cdot\mathbf{p}', \quad \mathbf{v}=\mathbf{m}^{-1/2}\cdot\mathbf{v}', \quad \mathbf{r}=\mathbf{m}^{-1/2}\cdot\mathbf{r}',\\ &\mathbf{E}=\mathbf{m}^{1/2}\cdot\mathbf{E}', \quad \mathbf{B}_0=|m|^{1/2}\mathbf{m}^{-1/2}\cdot\mathbf{B}_0',\\ &\mathbf{q}=\mathbf{m}^{1/2}\cdot\mathbf{q}', \quad \mathbf{J}=\mathbf{m}^{-1/2}\cdot\mathbf{J}',\end{aligned} \tag{4.5}$$

reduce the Boltzmann equation to the same form as for spherical energy surfaces. Therefore, the solutions to the Boltzmann equation in terms of the primed quantities are identical to the solutions for particles with isotropic mass. The conductivity tensor for the ellipsoidal case then may be obtained from the tensor appropriate to the spherical case by performing the inverse transformations. Hence, the ellipsoidal case can be discussed using (4.2) if $\mathbf{v}_F$, $\mathbf{q}$, $\mathbf{B}_0$, $\mathbf{E}$, and $\mathbf{J}$ are replaced by the corresponding primed quantities. The cyclotron frequency, which depends on the orientation of $\mathbf{B}_0$, is given by $\omega_c=eB_0'$. The tensor $\mathbf{m}^{1/2}$ is defined in the principal axes coordinate system of the ellipsoid by

$$\mathbf{m}^{1/2}=\begin{bmatrix} m_1^{1/2} & 0 & 0\\ 0 & m_2^{1/2} & 0\\ 0 & 0 & m_3^{1/2}\end{bmatrix}. \tag{4.6}$$

For PbTe, which has four $\langle 111\rangle$ prolate ellipsoids located at the Brillouin-zone boundaries, $m_1=m_2=m_t$ and $m_3=m_l=Km_t$.

In (4.2) there is a pole in the integrand arising from each term in the series. In the collisionless limit the Hermitian part of $\boldsymbol{\sigma}$ arising from the residues at the poles represents a resonant absorption of energy by the electrons. For transmission of magnetoplasma waves, as opposed to acoustic experiments or surface impedance measurements, the resonant absorption is likely to be observed only for $n=0$ and $n=1$. This is because absorption due to one or both of these terms occurs first as the applied field is reduced from a large value, and the wave becomes heavily damped or changes its character entirely before the resonant condition is reached for the other terms of the series. The anti-Hermitian part of $\boldsymbol{\sigma}$ determines the dispersion or phase of the wave and is affected by the proximity of a singularity even when the resonant condition is not reached.

The $n=1$ resonance, known as Doppler-shifted cyclotron resonance,[3] requires that

$$\omega_c=\omega-q_z'v_z', \tag{4.7}$$

for some electrons on the Fermi surface. This condition may be rewritten in terms of the average velocity $\mathbf{v}_{av}$ as

$$\omega_c=\omega-\mathbf{q}'\cdot\mathbf{v}_{av}'=\omega-\mathbf{q}\cdot\mathbf{v}_{av}, \tag{4.8}$$

since $\mathbf{v}_{av}'$ is simply $v_z'\hat{z}'$ and since the transformation (4.5) leaves the scalar product invariant. The interpretation of (4.8) is that resonant absorption of energy occurs if some electrons, as they move through the wave, see a rotating electric field at a Doppler-shifted frequency equal to their cyclotron frequency.[3]

The $n=0$ resonance is the one with which we are concerned in the experiments on PbTe and is the Landau damping mentioned earlier. This interaction occurs with those Fermi-surface electrons for which

$$\omega=q_z'v_z'=\mathbf{q}'\cdot\mathbf{v}_{av}'=\mathbf{q}\cdot\mathbf{v}_{av} \tag{4.9}$$

is satisfied, that is, with those electrons whose average velocity along the direction of propagation matches the phase velocity of the wave.

In Fig. 9 the regions of the (ω,q) plane in which DSCR and Landau damping occur are shown. Two zero-order dispersion relations are plotted for varying magnetic field strength for helicons propagating at constant frequency and angle θ with respect to the magnetic field. In terms of the normalized coordinates

[22] A. L. McWhorter and J. N. Walpole (to be published).

of Fig. 9, the dispersion relation takes the form

$$\frac{\omega}{\omega_c}=\left(\frac{\omega^2 m_c}{ne^2\mu_0\bar{v}_m^2\cos\theta}\right)^{1/3}\left(\frac{q\bar{v}_m\cos\theta}{\omega_c}\right)^{2/3}, \tag{4.10}$$

where $m_c=eB_0/\omega_c$ is the cyclotron mass and $\bar{v}_m$ is the maximum average Fermi velocity in the z direction. (In a many-valley semiconductor the values of ω_c and $\bar{v}_m$ will in general be different for each ellipsoid.) For $(\omega^2 m_c/ne^2\mu_0\bar{v}_m^2\cos\theta)$ above a critical value of $\frac{1}{2}$, DSCR occurs first as the field is decreased. Below this value, Landau damping will occur first and may obscure the onset of DSCR. At sufficiently high fields a region of no resonant damping can always be reached since the initial slope of the dispersion relation is infinite. Curve A is plotted for the critical case and curve B corresponds to the case for the PbTe sample I-B with propagation along B_0 and parallel to the [001] axis.

The fact that (4.9) can be satisfied tells one nothing about the strength of the resonant damping, of course. Indeed, for spherical energy surfaces with $\mathbf{B}_0$ parallel to $\mathbf{q}$, Landau damping vanishes, and it has erroneously been thought[10] to vanish whenever $\mathbf{B}_0$ is parallel to $\mathbf{q}$ for any closed Fermi surface. However, it can be shown[9] for closed Fermi surfaces of general shape that the strength of the damping depends upon the energy gained from the electric field by a resonant particle over one complete cyclotron orbit. In the present experiments, which involve ellipsoidal energy surfaces with $\mathbf{q}$ not along a principal axis, the energy transfer is nonzero even for $\mathbf{B}_0$ parallel to $\mathbf{q}$. Quinn[23] first showed the existence of damping in this geometry by a quantum calculation of the conductivity tensor for ellipsoidal energy surfaces. In this connection it should be noted that Landau damping, which in the semiclassical treatment is associated with the $n=0$ resonant denominator in (4.2), is quantum mechanically an intra-Landau-level transition in the limit of small momentum transfer, while DSCR (the $n=1$ resonance) corresponds to an inter-Landau-level transition.

B. Nonlocal Calculations to Second Order in $1/B_0$

The dispersion relation obtained from Maxwell's equations with displacement current neglected is of the form

$$\begin{vmatrix} i\omega\mu_0\sigma_{xx}-q^2\cos^2\theta & i\omega\mu_0\sigma_{xy} & i\omega\mu_0\sigma_{xz}+q^2\cos\theta\sin\theta \\ i\omega\mu_0\sigma_{yx} & i\omega\mu_0\sigma_{yy}-q^2 & i\omega\mu_0\sigma_{yz} \\ i\omega\mu_0\sigma_{zx}+q^2\cos\theta\sin\theta & i\omega\mu_0\sigma_{zy} & i\omega\mu_0\sigma_{zz}-q^2\sin^2\theta \end{vmatrix}=0. \tag{4.11}$$

in a coordinate system in which $\mathbf{z}\|\mathbf{B}_0$, $q_z=q\cos\theta$ and $q_x=q\sin\theta$. Here the σ_{ij} are the elements of the conductivity tensor *including* relaxation to the local equilibrium, i.e., the quantities denoted by σ_{ij}' in Ref. 20. In the local limit (4.11) has two roots, one of which corresponds to the helicon mode and the other to a highly attenuated cutoff mode.[24] Although new roots to (4.11) may exist in principle in the nonlocal regime, the helicon wave remains as the only propagating mode if ω/ω_c, $1/\omega_c\tau$, and qv_F/ω_c are all small.[25]

Second-order corrections to the helicon root of (4.11) may be obtained by expanding the components of $\boldsymbol{\sigma}$ to third order in $1/B_0$ with the parameters ω/ω_c, $1/\omega_c\tau$, and qv_F/ω_c considered as small quantities. The only component of $\boldsymbol{\sigma}$ which can have a term independent of B_0 is σ_{zz}. The Onsager relations require $\sigma_{ij}(B_0)=\sigma_{ji}(-B_0)$, and from the symmetry of the geometry chosen, the conductivity tensor must be invariant to reflection in the xz plane. It follows from these considerations that the expansion of the conductivity components in powers of $1/B_0$ to third order must have the following form:

$$\begin{aligned} &\sigma_{xx}=\sigma_{xx}^{(2)}, \quad \sigma_{yy}=\sigma_{yy}^{(2)}, \\ &\sigma_{xy}=-\sigma_{yx}=\sigma_{xy}^{(1)}+\sigma_{xy}^{(3)}, \\ &\sigma_{yz}=-\sigma_{zy}=\sigma_{yz}^{(1)}+\sigma_{yz}^{(3)}, \\ &\sigma_{xz}=\sigma_{zx}=\sigma_{xz}^{(2)}, \\ &\sigma_{zz}=\sigma_{zz}^{(0)}+\sigma_{zz}^{(2)}. \end{aligned} \tag{4.12}$$

In (4.12) the numerals in parentheses denote the order in $1/B_0$.

Using (4.12) in (4.11) and keeping only the terms which give corrections to q_0 of first and second orders in $1/B_0$, we obtain a dispersion relation of the form

$$q\approx q_0\left[1+\frac{\eta_1(q)}{B_0}+\frac{\eta_2(q)}{B_0^2}\right], \tag{4.13}$$

where

$$\frac{\eta_1(q)}{B_0}=\frac{i}{4\cos\theta}\left[\frac{\sigma_{xx}^{(2)}+\cos^2\theta\sigma_{yy}^{(2)}}{\sigma_{xy}^{(1)}}+\frac{(\cos\theta\sigma_{yz}^{(1)}-\sin\theta\sigma_{xy}^{(1)})^2}{\sigma_{xy}^{(1)}\sigma_{zz}^{(0)}}\right]$$

and

$$\begin{aligned} \frac{\eta_2(q)}{B_0^2}=&-\frac{1}{2}\left(\frac{\eta_1(q)}{B_0}\right)^2+\frac{\sigma_{xx}^{(2)}}{4\sigma_{zz}^{(0)}}\left[\left(\frac{\sigma_{yz}^{(1)}}{\sigma_{xy}^{(1)}}\right)^2-\tan^2\theta\right] \\ &+\frac{\sigma_{xx}^{(2)}\sigma_{yy}^{(2)}}{4(\sigma_{xy}^{(1)})^2}+\frac{\sigma_{xy}^{(3)}}{\sigma_{xy}^{(1)}}+\frac{\sigma_{xz}^{(2)}}{2\sigma_{zz}^{(0)}}\left[\frac{\sigma_{yz}^{(1)}}{\sigma_{xy}^{(1)}}-\tan\theta\right]. \end{aligned} \tag{4.14}$$

[23] J. J. Quinn, Phys. Rev. **135**, A181 (1964).
[24] C. R. Legendy, Phys. Rev. **135**, 1713 (1964).
[25] Transmission due to single-particle excitations (as opposed to collective modes such as the helicon wave) may occur in the nonlocal regime, but is negligible here since the sample thickness is much larger than the particle mean free path.

The first-order correction $\eta_1(q)/B_0$ contains the main features of the band structure and nonlocal corrections. The second-order term $\eta_2(q)/B_0^2$ is important only in obtaining a more exact evaluation of the imaginary part of q, since the zeroth-order expression gives no damping as previously mentioned.

The remaining problem in finding the dispersion relation is the calculation of the terms of the expansion in $1/B_0$ of the components of $\boldsymbol{\sigma}$. Four contributions to each term must be calculated, one from each ellipsoid. As the first step, the expansion of the isotropic mass conductivity tensor was obtained in powers of $1/B_0$. The transformations (4.5) were then applied for each ellipsoid and the results added together in a common coordinate system. After the final expressions were substituted into (4.13), q was evaluated iteratively by computer using q_0 as an initial approximation.[26]

Since the algebraic manipulations are lengthy though straightforward, we shall omit the details, which may be found elsewhere.[27] The results of the expansion of the components of the isotropic-mass conductivity tensor are given in Appendix A for reference. Although a similar expansion has been given before,[28] the results in Appendix A include relaxation to the local equilibrium. This effect is important in the case of a many-valley band structure since density fluctuations may occur on a per-ellipsoid basis even though the total density fluctuation is small (as we assume by neglecting displacement current). In order to treat each ellipsoid independently in this manner, the intervalley collision rate must be small compared to the frequency of the wave. This condition should be well satisfied in PbTe at 4.2°K. The additional terms that result from including relaxation to local equilibrium are numerically significant in both phase and amplitude for the conditions encountered in the present experiments.

Since the main features of the theoretical curves shown in Figs. 3–6 for $\mathbf{q}\|\mathbf{B}_0$ can be understood from the first-order corrections only, it may be useful to give for $\theta=0$ an explicit expression for (4.13) with second-order terms omitted:

$$q=q_0\left[1+\left(\frac{\omega}{2\omega_{ct}}-\frac{i}{2\omega_{ct}\tau}\right)\left(\frac{2K+1}{K+2}\right)-i\left(\frac{qv_{Ft}}{\omega_{ct}}\right)\left(\frac{3}{K+2}\right)^{1/2}\frac{(K-1)^2}{8(K+2)}G(a)\right], \tag{4.15}$$

where

$$G(a)=\left(1+\frac{1}{a^2}\right)^2\tan^{-1}a-\left(\frac{5}{3a}+\frac{1}{a^3}\right)+\frac{1}{a^3}\frac{[(a+1/a)\tan^{-1}a-1]^2}{1+i\omega\tau-(1/a)\tan^{-1}a} \tag{4.16}$$

and

$$a=\left[\left(\frac{3}{K+2}\right)^{\frac{1}{2}}qv_{Ft}\tau\right](1+i\omega\tau)^{-1}. \tag{4.17}$$

Here v_{Ft} is the Fermi velocity transverse to the axis of revolution of the ellipsoid and $\omega_{ct}=eB_0/m_t$. The last term in (4.16) results from including relaxation to local equilibrium. The theoretical curves in Figs. 3–6 were of course actually calculated using the full expression (4.13), including the second-order term $\eta_2(q)/B_0^2$. Also included in the numerical calculation was the magnetic field dependence of the excitation of the wave, which results from a $1/q$ variation in the coupling to the microwave signal in the waveguide. The theoretical curves marked L were also calculated from (4.13) by evaluating the $\sigma_{ij}^{(n)}$ at $q=0$.

V. COMPARISON OF THEORY AND EXPERIMENT

It is well established that the energy bands in PbTe are nonparabolic,[29] and probably the energy surfaces are not strictly ellipsoidal as well.[30] However, if we assume that the deviation from ellipsoidal shape is small, nonparabolicity may easily be included in the preceding treatment by allowing for a concentration dependence of the mass parameters. For a nonparabolic but ellipsoidal model the energy-momentum relation is[31]

$$E(1+E/E_g)=\sum_i p_i^2/2m_{i0}, \tag{5.1}$$

where p_i is the momentum component along the ith axis of the ellipsoid and m_{i0} is the band-edge mass parameter. It is assumed that the total energy E is small compared to the energy gap E_g between the interacting bands. For an ellipsoid of revolution, (5.1) leads to a fixed anisotropy ratio K and a transverse mass m_t which varies as

$$m_t=m_{t0}[1+cn^{2/3}], \tag{5.2}$$

where the constant c is given by

$$c=(3\pi^2\hbar^3/4\sqrt{K})^{2/3}/m_{t0}E_g \tag{5.3}$$

[26] A Taylor expansion of η_1 and η_2 about $q=q_0$ is not adequate because of the logarithmic singularities which occur in these functions.

[27] J. N. Walpole, Ph.D. thesis, Massachusetts Institute of Technology, 1966 (unpublished).

[28] S. G. Eckstein, Phys. Rev. 131, 1087 (1963).

[29] See, for example, K. F. Cuff, M. R. Ellett, C. D. Kuglin, and L. R. Williams, in *Proceedings of the Seventh International Conference on the Physics of Semiconductors, Paris, 1964* (Dunod Cie., Paris, 1964), p. 677.

[30] J. O. Dimmock and G. B. Wright, in *Proceedings of the Seventh International Conference on the Physics of Semiconductors, Paris, 1964* (Dunod Cie., Paris, 1964), p. 77.

[31] B. Lax and J. G. Mavroides, in *Solid State Physics*, edited by F. Seitz and D. Turnbull (Academic Press Inc., New York, 1960), Vol. 11, p. 261.

for the case of PbTe, which has four conduction-band ellipsoids.

As mentioned in Sec. III, data was obtained from samples of four different carrier concentrations. If it is assumed that m_t varies with concentration according to (5.2), m_{t0} and the constant c can be determined by adjusting these parameters to achieve a theoretical fit to the data for all four concentrations. The anisotropy ratio K is not a sensitive parameter in the theoretical expressions for fixed angle of propagation with respect to the field and it seems evident that anisotropic scattering prevents the determination of this parameter from the dependence on θ of the phase and amplitude. Hence no attempt was made to determine K; the value 10 was used throughout.[29,32]

The concentration is determined by the initial slope at high fields of the phase-shift curves (Figs. 3 and 4), and it is not possible to adjust n further in order to achieve a fit at lower fields. The anisotropy ratio K has little effect on the curvature of the phase plots at low fields for values of K within 20% of 10, nor has the value of $\omega\tau$ over a range from 0.1 to 10. However, a few percent change in m_t has a marked effect on the curvature, so that the transverse mass may be determined quite accurately from the low-field phase data. The sensitivity to m_t and the insensitivity to K arise from a competition between local and nonlocal terms. The tendency for the terms of the conductivity which are present in the local theory to give an upward curvature to the phase plot is offset by the additional terms which are present in the nonlocal regime and which produce a downward curvature. While reducing K reduces both the local and nonlocal terms in a roughly compensating fashion, the reduction of m_t increases the effect of the nonlocal terms and decreases the local one. This behavior may be seen from (4.15) since the local term to first order is proportional to (ω/ω_{ct}), which varies as m_t, and the nonlocal one depends on qv_{Ft}/ω_{ct} times a strong function of qv_{Ft}, which varies as $1/m_t$. The values of $\omega\tau$ used in the calculations were obtained by fitting the amplitude data for propagation along the magnetic field. Hence, no parameters were determined from the data for propagation at an angle to the field.

In summary, the anisotropy ratio K was taken as 10, the concentrations n were obtained from the initial slopes of the curves of phase shift vs $B_0^{-1/2}$, the parameters m_{t0} and c were adjusted to give a fit to the low-field curvature of the phase-shift plots for four concentrations, and the values of $\omega\tau$ were determined from the amplitude data.

The values thus found for m_{t0} and c were $m_{t0}=0.020m_0$ and $c=2.65\times10^{13}$ cm^2. The latter is 25% smaller than the theoretical result one would obtain using (5.3) and taking $E_g=0.19$ eV.[29] The discrepancy is not significant since we are using a very simple model for the interacting bands. The present value of m_{t0} is somewhat smaller than the previously estimated[29] one of 0.024 ± 0.003 m_0, but again the discrepancy is not very significant in view of the possible effects of nonellipsoidal energy surfaces and anisotropic scattering. Using the values of m_{t0} and c, we predict $m_t=0.022m_0$ for a concentration of 2×10^{17} cm^{-3}, which may be compared to the value 0.024 m_0 obtained by Nii[32] at the same concentration from cyclotron resonance data. The values found for $\omega\tau$ were about 2 (for sample *I-A*, $\omega\tau=1.9$; for sample *I-B*, $\omega\tau=2.0$).

The disagreement between theory and experiment for the change in amplitude with the angle of the magnetic field in Fig. 7 and 8 is believed to be due to anisotropic scattering. Allgaier's[33] dc galvonomagnetic experiments on PbTe at 4.2°K have given values of $K'=m_l\tau_t/m_t\tau_l$ ranging from 4 to 6, which implies an anisotropy τ_l/τ_t of the order of 2 since $K=m_l/m_t$ is about 10. For sample *I-A*, which has the lowest concentration, a first-order perturbation calculation in the local limit[22] yields for $\tau_l/\tau_t=2$ a correction to the angular dependence of the amplitude which is of the right size to account for the discrepancy in Fig. 8. Little effect of collision anisotropy on the phase of the helicon wave is predicted. A confirmation of the role of anisotropic collisions will require experiments at higher fields where second-order terms and nonlocal effects can be completely neglected or else extending the theory for anisotropic scattering beyond the first-order perturbation treatment.

VI. DISCUSSION AND CONCLUSIONS

As seen in Figs. 3–8, the phase data is in good agreement with the theory, as is the attenuation for propagation along the field. However, the angular dependence of the attenuation strongly suggests that anisotropic collisions are present. When θ is fixed, collision anisotropy is probably not of great importance since the main effect can be taken into account by an effective collision time. Nevertheless, without a full treatment of the collision effects the mass anisotropy cannot be determined with any precision from the data. The transverse mass, on the other hand, is a sensitive parameter in the theoretical behavior of the phase shift in either the local or nonlocal regimes. The low-field helicon experiment provides a good measurement of this quantity, within the assumption of ellipsoidal energy surfaces. In fact, in the nonlocal regime the helicon problem is more tractable theoretically than cyclotron resonance since nonlocal effects may be taken into account as small corrections. Except in the extreme anomalous limit of Azbel-Kaner cyclotron resonance, the treatment of cyclotron resonance under nonlocal conditions is quite difficult.

In the concentration range of these experiments the nonlocal effects vary from nearly negligible ones at the

[32] R. Nii, J. Phys. Soc. Japan **19**, 58 (1964).

[33] R. S. Allgaier, Phys. Rev. **112**, 828 (1958).

lowest concentration ($n=1.7\times10^{17}$ cm^{-3}) to extremely important ones at the highest concentration ($n=8.1\times10^{17}$ cm^{-3}). This behavior is easily understood in terms of the parameter qv/ω_c, which is proportional to $n^{5/6}$, if we use q_0 for q. Hence for heavier concentrations the dispersion relation lies further into the cross-hatched region of Landau damping in Fig. 9 for a given value of ω/ω_c.

It should be pointed out again that relaxation to the local equilibrium can be important in a many-valley band structure because of fluctuations in the individual ellipsoid populations. Such fluctuations can exist when the intervalley collision rate is long, even though the total density fluctuation is zero as for transverse waves in general, or quite small as in the helicon wave with negligible displacement current.

The experimental results for propagation along the field confirm the semiclassical theory for the nonlocal regime in some detail for a relatively simple yet highly interesting model. Striking nonlocal effects are produced by Landau damping, which can occur even for propagation along the field because of the anisotropic energy surfaces in PbTe. Although the presence of Landau damping does not necessarily have a strong influence on the helicon wave, since the interaction can be arbitrarily weak depending on the shape of the Fermi surface and the value of qv_F/ω_c, it would nevertheless appear that phase shift and attenuation of helicons in materials with general energy surfaces would not be interpretable in terms of DSCR interaction only.

ACKNOWLEDGMENTS

The authors wish to thank A. R. Calawa, A. J. Strauss and R. F. Brebrick for discussion and assistance with sample preparation and annealing procedures; W. G. May for many helpful suggestions concerning experimental techniques; and Mrs. Billie H. Houghton for the computer calculations.

APPENDIX A: EXPANSION OF THE CONDUCTIVITY TENSOR IN POWERS OF $1/B_0$

The components of the isotropic-mass conductivity tensor may be expanded in powers of $1/B_0$ when $|(\omega-i/\tau)/\omega_c|<1$ and $qv_F/\omega_c<1$. In the absence of density fluctuations, we simply expand in (4.2) the Bessel functions and the factors $(n\omega_c-\omega+q_zv_F\cos\theta+i/\tau)^{-1}$ for $n\neq0$ in a power series in $1/\omega_c$ before carrying out the integration over θ. With density fluctuations, the requirement of relaxation to the local equilibrium gives additional terms in the expansion of the components. However, these additional terms are related through an Einstein relation[20] to those derived from (4.2). The calculations are straightforward but tedious; we give here only the results. For $\mathbf{q}$ in the xz plane and with the z axis parallel to $\mathbf{B}_0$, we obtain to lowest order in $1/B_0$

$$\frac{\sigma_{xx}}{\sigma_0}\approx\frac{\sigma_{xx}^{(2)}}{\sigma_0}=\frac{1+i\omega\tau}{(\omega_c\tau)^2},$$

$$\frac{\sigma_{yy}}{\sigma_0}\approx\frac{\sigma_{yy}^{(2)}}{\sigma_0}=\frac{1+i\omega\tau}{(\omega_c\tau)^2}\left\{1+\frac{3}{4}\left(\frac{q_x}{q_z}\right)^2\left[a(1+1/a^2)^2\tan^{-1}a-(5/3+1/a^2)\right]+\frac{3}{4}\left(\frac{q_x}{q_z}\right)^2\frac{1}{a^2}\frac{[(a+1/a)\tan^{-1}a-1]}{1+i\omega\tau-(1/a)\tan^{-1}a}\right\},$$

$$\frac{\sigma_{zz}}{\sigma_0}\approx\frac{\sigma_{zz}^{(0)}}{\sigma_0}=\left(\frac{3i\omega\tau}{1+i\omega\tau}\right)\frac{1}{a^2}\left[\frac{1-(1/a)\tan^{-1}a}{1+i\omega\tau-(1/a)\tan^{-1}a}\right],$$

$$\frac{\sigma_{xy}}{\sigma_0}\approx\frac{\sigma_{xy}^{(1)}}{\sigma_0}+\frac{\sigma_{xy}^{(3)}}{\sigma_0}=-\frac{1}{\omega_c\tau}+\frac{(1+i\omega\tau)^2}{(\omega_c\tau)^3}\left\{1+\frac{1}{2}\left(\frac{q_x}{q_z}\right)^2\frac{[(a+1/a)\tan^{-1}a-1]}{1+i\omega\tau-(1/a)\tan^{-1}a}+\left[\frac{3}{10}\left(\frac{q_x}{q_z}\right)^2-\tfrac{1}{5}\right]a^2\right\},$$

$$\frac{\sigma_{yz}}{\sigma_0}\approx\frac{\sigma_{yz}^{(1)}}{\sigma_0}=-\frac{1}{\omega_c\tau}\left(\frac{q_x}{q_z}\right)\left\{1-i\frac{3\omega\tau}{2a^2}\frac{[(a+1/a)\tan^{-1}a-1]}{1+i\omega\tau-(1/a)\tan^{-1}a}\right\},$$

$$\frac{\sigma_{xz}}{\sigma_0}\approx\frac{\sigma_{xz}^{(2)}}{\sigma_0}=-\frac{q_x}{q_z}\frac{1+i\omega\tau}{(\omega_c\tau)^2}\left[\frac{1-(1/a)\tan^{-1}a}{1+i\omega\tau-(1/a)\tan^{-1}a}\right], \tag{A1}$$

where

$$\sigma_0=ne^2\tau/m \tag{A2}$$

and

$$a=(q_zv_F\tau)/(1+i\omega\tau). \tag{A3}$$

The numerals in parentheses indicate the order in $1/B_0$ of the component. Note that for σ_{xy} we have included the next higher nonvanishing term $\sigma_{xy}^{(3)}$, since this term is required in order to obtain $(\Delta q/q_0)$ to second order in $1/B_0$ for the helicon wave.